(Title) Altered Fhod3 Expression Involved in Progressive High-Frequency Hearing Loss via Dysregulation of Actin Polymerization Stoichiometry in The Cuticular Plate

Ely Boussaty[1]*, Yuzuru Ninoyu[1]*, Leo Andrade[2], Qingzhong Li[3], Takahiro Ohyama[3], Karl J Wahlin[4], Uri Manor[2,5]†, Rick A Friedman[1]†

1. Department of Otolaryngology – Head and Neck Surgery, University of California, San Diego, La Jolla, CA, USA
2. Waitt Advanced Biophotonics Center, Salk Institute for Biological Studies, La Jolla, CA, USA
3. USC-Tina and Rick Caruso Department of Otolaryngology-Head & Neck Surgery, Zilkha Neurogenetic Institute, USC Keck School of Medicine, University of Southern California, Los Angeles, USA
4. Shiley Eye Institute, University of California, San Diego, San Diego, CA, USA
5. Department of Cell & Developmental Biology, School of Biological Sciences, University of California, San Diego, USA

* These authors contributed equally to this work.

† Corresponding author:
Rick A Friedman (rafriedman@health.ucsd.edu), Uri Manor(urimanor@ucsd.edu)

Running title: Fhod3 regulates actin dynamics in the cochlea

Keywords: Age-related hearing loss (ARHL), Genome-wide association studies (GWAS), hair cells, actin, stereocilia, Multiplexed error-robust fluorescence in situ hybridization (MERFISH)

Number of words: 50430 words

Number of figures: 5

Abstract

Age-related hearing loss (ARHL) is a common sensory impairment with comlex underlying mechanisms. In our previous study, we performed a meta-analysis of genome-wide association studies (GWAS) in mice and identified a novel locus on chromosome 18 associated with ARHL specifically linked to a 32 kHz tone burst stimulus. Consequently, we investigated the role of Formin Homology 2 Domain Containing 3 (Fhod3), a newly discovered candidate gene for ARHL based on the GWAS results. We observed Fhod3 expression in auditory hair cells (HCs) and primarily localized at the cuticular plate (CP). To understand the functional implications of Fhod3 in the cochlea, we generated Fhod3 overexpression mice (*Pax2-Cre*$^{+/-}$*; Fhod3*$^{Tg/+}$) (TG) and HC-specific conditional knockout mice (*Atoh1-Cre*$^{+/-}$*; Fhod3*$^{fl/fl}$) (KO). Audiological assessments in TG mice demonstrated progressive high-frequency hearing loss, characterized by predominant loss of outer HCs and decrease phalloidin intensities of CP. Ultrastructural analysis revealed shortened stereocilia in the basal turn cochlea. Importantly, the hearing and HC phenotype in TG mice were replicated in KO mice. These findings indicate that Fhod3 plays a critical role in regulating actin dynamics in CP and stereocilia. Further investigation of Fhod3-related hearing impairment mechanisms may facilitate the development of therapeutic strategies for ARHL in humans. (198 words)

1 Introduction

Age-related hearing loss (ARHL) is one of the most common causes of sensorineural hearing loss among the elderly population. Numerous studies have identified candidate genes associated with ARHL, implicating molecular pathways such as oxidative stress response (Sugiura et al. 2010; Someya et al. 2010), inflammation (Rodríguez-de la Rosa et al. 2017; Menardo et al. 2012), and cellular senescence (Benkafadar et al. 2019; Li et al. 2022). However, due to the polygenic nature (Fransen et al. 2015) and phenotypic heterogeneity of ARHL (Gates and Mills 2005), the underlying mechanisms have not been fully elucidated. Further investigation is necessary to facilitate targeted interventions and personalized treatment approaches for ARHL.

Genome-wide association studies (GWAS) have been conducted in humans to explore the genetic architecture of ARHL and have successfully identified loci significantly associated with ARHL susceptibility (Friedman et al. 2009; Van Laer et al. 2010). However, GWAS studies often explain only a fraction of the heritability of complex traits, indicating the presence of undiscovered genetic variants contributing to ARHL. This may be attributed to limitations in study design, sample size, or the influence of rare variants that are challenging to detect. To address these challenges, we performed GWAS on a cohort of approximately 100 extensively characterized inbred mouse strains, known as the hybrid mouse diversity panel (HMDP) (Ghazalpour et al. 2012).This robust resources enables the investigation of both genetic and environmental influences on intricate traits. Our study successfully identified distinct genetic and phenotypic differences, expanding upon the known Mendelian ARHL genes (Ahl) described to date (Lavinsky et al. 2015; Ohmen et al. 2014). The mouse model provides a valuable platform for studying the genetics of hearing loss, as the mouse and human ears are functionally and

71 genetically homologous, allowing for the translation of findings to human populations
72 (Ghazalpour et al. 2012; Flint and Eskin 2012; Rau et al. 2015). However, additional studies are
73 required to fully understand how the identified variants influence the ARHL phenotype.
74 The loss of cochlear HCs and their associated mechanoelectrical transduction function
75 significantly contributes to the development of ARHL (Schuknecht and Gacek 1993). HCs,
76 specialized sensory cells within the inner ear, possess stereocilia, tiny hair-like structures
77 arranged in a staircase pattern. Each stereocilium consists of a bundle of actin filaments, tightly
78 regulated in length and anchored into a cuticular plate or dense actin meshwork at their base.
79 Actin-regulatory proteins play a crucial role in maintaining the fine actin structure, and mutations
80 in these proteins have been associated with various forms of hereditary hearing loss(Miyoshi et
81 al 2021). However, the precise role of actin-regulatory proteins in ARHL remains unclear.
82 Rho-GTPases, such as cell division cycle 42 (Cdc42) and RhoA, are well-known actin-regulatory
83 proteins that play a pivotal role in regulating actin dynamics in HCs (Ueyama et al 2014;
84 Anttonen et al. 2017). Formin proteins that function as downstream effectors of RhoA are
85 involved in regulating multiple cellular actin cytoskeletal elements by nucleating and
86 polymerizing straight actin filaments (Breitsprecher and Goode 2013). While the Diaphanous-
87 related formin family (DRF) members DIAPH1 (Lynch et al. 1997) and DIAPH3 (Sánchez-
88 Martínez et al. 2017; Schoen et al. 2010) are known hereditary hearing loss-related proteins, the
89 physiological role of other DRF proteins in the HC, such as FHOD, have yet to be fully
90 established.
91 FHOD3, initially described in the regulation of sarcomere organization in cardiomyocytes, has
92 been localized to thin actin filaments with abundant expression in both myocardium and skeletal
93 muscle (Taniguchi et al. 2009). Depletion of FHOD3 leads to a reduction of filamentous actin

94 and disruption of sarcomere organization in cardiac cells (Taniguchi et al. 2009). Studies have
95 shown that FHOD3 is involved in actin polymerization and myofibril integrity (Kan-O et al.
96 2012). Interestingly, FHOD3 has been observed at the pointed ends of actin filaments, where
97 depolymerization normally occurs, suggesting a potential role in annealing short actin filaments
98 (Fujimoto et al. 2016).
99 In this study, we aimed to investigate the functional implications of Fhod3, a novel candidate
100 gene for ARHL identified through meta-analysis GWAS in mice. We generated two mouse
101 models: Fhod3 overexpression mice (*Pax2-Cre*$^{+/-}$*; Fhod3*$^{Tg/+}$) and HC-specific conditional
102 knockout mice (*Atoh1-Cre*$^{+/-}$*; Fhod3*$^{fl/fl}$). Audiological assessments in the transgenic mice
103 revealed a progressive high-frequency hearing loss phenotype, accompanied by the predominant
104 loss of outer HCs and deterioration of the cuticular plate. Scanning electron microscopy analysis
105 demonstrated shortened stereocilia, particularly in the mid-base and base regions of the cochlea.
106 Furthermore, targeted deletion of Fhod3 replicated the progressive hearing loss and HC
107 deterioration observed in the Fhod3 overexpression mutants. These findings suggest a critical
108 role for Fhod3 in regulating actin dynamics in the cuticular plate and stereocilia of high-
109 frequency cochlear hair cells.
110

111 **2. Results**

112

113 **2.1 Random effects meta-analysis GWAS identifies 5 loci for ARHL in mice**

114 Mouse strains exhibit higher heritability for complex traits, and the genetic loci associated with
115 these traits tend to exert stronger effects compared to humans. Motivated by these advantages,
116 we performed the first GWAS of its kind in the mouse by combining several data sets in a meta-

117 analysis to identify loci associated with ARHL (Ohmen et al. 2014). We identified five genome-
118 wide significant loci (P<1.0x10^{-6}). One of these confirmed a previously identified locus (*Ahl8*)
119 on distal chromosome 11 and greatly narrowed the candidate region. Another locus of interest
120 appeared for the 32 kHz tone burst stimulus and localized to chromosome 18 with the peak SNP
121 (position 24320393; P=2.32 x 10^{-6}) appearing within a haplotype block between 24.25 and 25.65
122 Mb containing the formin-like gene *Fhod3* (Ohmen et al. 2014). Due to its role in actin
123 polymerization/capping, we decided to delve into the potential role of *Fhod3* in high-frequency
124 and progressive hearing loss.
125

126 **2.2 Spatial expression patterns of Fhod3 mRNA and protein in the cochlea.**

127 To analyze the gene expression patterns of Fhod3 in the inner ear, we employed multiplexed
128 error-robust fluorescence in situ hybridization (MERFISH) (Chen et al. 2015) in P5 cochlea. The
129 application of single-molecule imaging allowed us to visualize Fhod3 expression in auditory
130 HCs and SGNs of the cochlea with high resolution (Fig. 1A to C). Additionally, we conducted
131 immunofluorescence staining in P5 cochleae to further confirm the localization of Fhod3. Our
132 results revealed the expression of Fhod3 in both outer HCs (OHCs), inner HCs (IHCs), and in
133 SGNs (Fig. 1C). We generated a conditional knock-out mouse model targeting Fhod3
134 specifically in HCs using Atoh1-cre and Fhod3-flox mice. In these knock-out mice (*Atoh1-*
135 *Cre*$^{+/-}$*; Fhod3*$^{fl/fl}$), Fhod3 signals were absent in HCs but still observed in SGNs, verifying Fhod3
136 expression in the cochlea (Fig.1C). Furthermore, to gain insights into the subcellular localization
137 of Fhod3 within HCs, we developed a Fhod3-HA tagged knock-in mouse model (Fhod3$^{HA/+}$) in
138 which a 3xHA sequence was inserted into the C-terminus of Fhod3 prior to the stop codon. This
139 demonstrated that Fhod3 predominantly localized to the cuticular plate in HCs (Fig.1D and E).

140 Supporting these findings, data obtained from gEAR.org (https://umgear.org/) corroborates the
141 high enrichment of Fhod3 expression specifically in cochlear HCs.
142

143 **2.3 Generation of a transgenic mouse model overexpressing Fhod3**

144 In our meta-analysis GWAS, the largest sample set utilized backcross data with C57/Bl6 (B6)
145 and DBA/2J (D2) strains to map *Ahl8* (Ohmen et al. 2014). Considering the hearing effect
146 observed in our meta-analysis, we aimed to investigate the potential differential expression of
147 *Fhod3* as a plausible mechanism. Through quantitative PCR (qPCR) analysis, we found
148 significantly higher levels of Fhod3 mRNA in D2 cochleae, a model of early-onset progressive
149 hearing loss (B6 vs D2; 1.07 ± 0.088 vs 2.00 ± 0.643, p^{**}=0.0079 by Mann-Whitney U test)
150 (Fig. 2A). These findings led us to hypothesize that *Fhod3* expression variation might contribute
151 to hearing loss. To further explore this hypothesis, we sequenced the *Fhod3* clone obtained from
152 B6 cochleae and identified three missense mutations (A1888C/rs29670988, C2232T/rs13483257,
153 and G2730A/rs30077504) as well as four synonymous polymorphisms in the D2 allele (Fig.2B).
154 Although the coding variations in the D2 allele were not predicted to be deleterious by PolyPhen
155 and SIFT software, we postulated that the hearing loss phenotype could still be associated with
156 this region, possibly due to *Fhod3* overexpression in D2. To investigate this possibility, we
157 generated a transgenic mouse model by introducing the full-length Fhod3 cloned from B6
158 cochleae between loxP-flanked stop cassettes and IRES-GFP, allowing tissue-specific Fhod3
159 overexpression in vivo (Fig.2C). Two transgenic mouse lines were obtained and subsequently
160 crossed with a B6 Pax2-Cre driver line (Ohyama and Groves 2004) to induce Fhod3
161 overexpression in the developing inner ear epithelium. The resulting offspring carrying both the
162 *Fhod3* allele and *Pax2-Cre* genes ($Pax2\text{-}Cre^{+/-}$; $Fhod3^{Tg/+}$) exhibited normal survival and did not

163 display any gross morphological phenotype. Through qPCR and immunofluorescence, we
164 observed elevated levels of Fhod3 mRNA (WT vs TG; 1.00 ± 0.311 vs 5.84 ± 0.821, p^{**}=0.0095
165 by Mann-Whitney U test) (Fig. 2D) and of FHOD3 protein expression in the mutant cochlea
166 (Fig. 2E).
167

168 **2.4 Inner ear specific *Fhod3* overexpression leads to progressive high-frequency hearing**
169 **loss with outer hair cell dominant HC loss and cuticular plate deterioration.**

170 To assess the auditory function of the Fhod3 transgenic mice (*Pax2-Cre*$^{+/-}$; *Fhod3*$^{Tg/+}$), auditory
171 brainstem responses (ABR) were measured at 6 and 12 weeks postnatally. The mutant mice
172 demonstrated a progressive elevation of ABR thresholds specifically at 24 kHz and 32 kHz
173 frequencies [WT vs TG: (6 weeks) 26.7 ± 1.47 vs 38.3 ± 6.91 dB at 24kHz, p= 0.0097, 42.1 ±
174 7.72 vs 64.6 ± 3.97 at 32 kHz, p<0.0001; (12 weeks) 25.0 ± 1.01 vs 46.25 ± 5.99 dB at 24 kHz,
175 p<0.0001, 42.9 ± 5.28 vs 75.4 ± 2.13 dB at 32 kHz, p<0.0001] (Fig. 3A). Corresponding to the
176 threshold elevation, histological examination revealed HC loss predominantly in the OHCs
177 within the region associated with high frequencies at 5 months old (Fig. 3B). The OHC survival
178 rate in the TG mice was significantly decreased at the basal turn region compared to WT mice
179 (WT vs TG (%): (IHC)100 vs 100 at apical turn (Api), 98.7 ± 0.95 vs 97.7 ± 1.51 at middle turn
180 (Mid), 94.7 ± 2.24 vs 85.9 ± 6.90 at basal turn (Base); (OHC) 97.1 ± 1.16 vs 95 ± 2.56 at Api,
181 96.8 ± 0.36 vs 96.5 ± 1.42 at Mid, 95.6 ± 0.64 vs 75.93 ± 8.98 at base, p^{*}=0.0233 by two-way
182 ANOVA followed by a Tukey post-hoc test) (Fig. 3C). Additionally, a significant reduction in
183 phalloidin intensity at the cuticular plate, a critical structure composed of a dense actin
184 meshwork, was observed in OHCs at the mid-basal turn (WT vs TG: (IHC)1.00 ± 0.175 vs 0.92

185 ± 0.179; (OHC)1.00 ± 0.131 vs 0.70 ± 0.170, $p^{***}<0.001$, by Mann-Whitney U test). (Fig. 3D
186 and E). These findings strongly suggest that increased Fhod3 expression reduces HC integrity,
187 leading to progressive hearing loss through HC loss.
188

189 **2.5 FHOD3 overexpression deteriorated the third row of stereocilia of the hair cells in**
190 **the base of the cochlea.**

191 To investigate the impact of Fhod3 overexpression on stereocilia, we conducted an
192 ultrastructural analysis using scanning electron microscopy on transgenic mice (TG) (*Pax2-*
193 *Cre*$^{+/-}$*; Fhod3*$^{Tg/+}$) in comparison to wild-type mice (WT) (*Pax2-Cre*$^{-/-}$*; Fhod3*$^{Tg/+}$) at 7 weeks of
194 age. Our examination revealed a significant decrease in the number of stereocilia in the shortest
195 (third) row of both inner and outer hair cells within the basal regions of the cochlea in the TG
196 mice (Fig. 4). These findings, combined with our localization data demonstrating Fhod3
197 presence in the cuticular plate (Fig. 1E and F), indicate that FHOD3 plays a crucial role in
198 maintaining actin dynamics within the stereocilia of both IHCs and OHCs via the cuticular plate.
199

200 **2.6 Targeted deletion of *Fhod3* induced progressive hearing loss and hair-cell**
201 **deterioration.**

202 Constitutive knockout of Fhod3 in mice results in prenatal lethality, likely due to developmental
203 defects in the myocardium(Ushijima et al. 2018). Therefore, to gain deeper insights into the
204 specific impact of Fhod3 deficiency on the mouse cochlea, it was crucial to achieve tissue-
205 specific inactivation of Fhod3. To accomplish this, we generated mice with a floxed allele of
206 Fhod3 combined with a Atoh1 promoter-driven Cre construct, enabling HC-specific Fhod3
207 inactivation. Remarkably, these mutant mice exhibited a physiological phenotype similar to that

208 of Fhod3 overexpression mutants, characterized by elevated auditory brainstem response (ABR)
209 thresholds specifically at the highest frequencies of 24 kHz and 32 kHz [WT vs KO: (6 weeks)
210 34.25 ± 4.12 vs 36.2 ± 2.83 dB at 24kHz, 36.3 ± 5.03 vs 50.1 ± 6.35 at 32 kHz, p^{**}=0.0096; (12
211 weeks) 32.3 ± 1.20 vs 52.9 ± 5.80 dB at 24 kHz, p^{**}=0.0031, 39.0 ± 4.51 vs 73.5 ± 4.55 dB at
212 32 kHz, p^{***}<0.0001; (18 weeks) 34.9 ± 2.93 vs 53.8 ± 3.06 dB at 24kHz, p^{*}= 0.0187, 51.4 ±
213 4.91 vs 80.8 ± 3.74 at 32 kHz, p^{***}<0.0001] (Fig. 5A). Importantly, the observed high-
214 frequency hearing loss progressed over time and heterozygous (Het) mice also showed threshold
215 elevation in the high frequency. [Het: (6 weeks) 41.8 ± 6.53 dB at 24kHz, 54.3 ± 5.43 at 32 kHz,
216 p^{*}=0.0179 (vs WT); (12 weeks) 47.0 ± 9.42 dB at 24 kHz, 72.4 ± 6.29 dB at 32 kHz,
217 p^{***}<0.0001 (vs WT); (18 weeks) 67.3 ± 13.6 dB at 24kHz, p^{***}= 0.0002 (vs WT), 86.0 ± 4.86
218 at 32 kHz, p^{***}<0.0001(vs WT)]. Additionally, we observed a significant increase in hair cell
219 loss in the basal turn of the cochlea at 3 months of age in KO mice (Fig. 5B), along with a
220 notable reduction in phalloidin intensity in IHCs and OHCs at the cuticular plate in the mid-basal
221 turn of the cochlea (WT vs KO: (IHC)1.00 ± 0.037 vs 0.96 ± 0.005, p^{*}=0.035; (OHC)1.00 ±
222 0.023 vs 0.67 ± 0.017, p^{***}<0.001 by Mann-Whitney U test) (Fig. 5C), consistent with our
223 findings in the transgenic overexpression mice (Fig. 3E). Scanning electron microscopy analysis
224 similarly revealed fused, shortened, and missing stereocilia in the mid-base of the cochlea,
225 corresponding to the tonotopic region associated with hearing loss (Fig. 5E). These results
226 indicate that alterations in Fhod3 expression levels, whether elevated or reduced, disrupt the
227 stoichiometry of actin polymerization at the cuticular plate, primarily affecting the HCs of the
228 third row stereocilia in the mid-basal and basal regions of the cochlea.
229
230 **3. Discussion**

231 Here we provide compelling evidence for the crucial role of Fhod3, identified through a meta-
232 analysis of GWAS for age-related hearing loss (ARHL), in maintaining auditory function. Using
233 genetic and molecular approaches, we demonstrated that altered expression of Fhod3 leads to
234 progressive high-frequency dominant hearing loss in two different mouse models: *Pax2-Cre*$^{+/-}$;
235 *Fhod3*$^{Tg/+}$ and *Atoh1-Cre*$^{+/-}$; *Fhod3*$^{fl/fl}$. Moreover, we observed the deterioration of the cuticular
236 plate and the shortest row of stereocilia in the mutant mice, indicating that dysregulation of
237 Fhod3 disrupts actin turnover balance and affects the integrity of cochlear HCs. This disruption
238 results in the loss of OHCs and could be a potential mechanism underlying ARHL.
239
240 In our previous meta-analysis GWAS, which mainly involved C57BL/6J (B6) and DBA/2J (D2)
241 F1 intercross data, we identified five genome-wide significant loci associated with ARHL in
242 mice (Ohmen et al. 2014). In this study, we focused on investigating the potential involvement of
243 Fhod3 in high-frequency and progressive hearing loss, despite the presence of several other
244 candidate genes within the 1Mb interval of the haplotype block. Although we did not find
245 deleterious Fhod3 polymorphisms in the D2 strain (Fig.2B), quantitative PCR revealed
246 significantly higher inner ear expression of Fhod3 in D2 compared to B6 (Fig.2A). Furthermore,
247 Fhod3 mRNA was detected in the human inner ear transcriptome (Schrauwen et al. 2016),
248 supporting its role in human hearing. We subsequently demonstrated that overexpression of
249 Fhod3 in the inner ear leads to high-frequency hearing loss in transgenic mice, accompanied by
250 sparse actin meshwork in the cuticular plate and loss of the shortest row of stereocilia in specific
251 cochlear turn. Notably, mice with P264L gamma actin mutations exhibited a similar phenotype
252 of stereocilia loss (Drummond et al. 2012). While mutations in Fascin Actin-Bundling Protein 2
253 (Fscn2) were implicated in mid-high frequency hearing loss in D2 mice, they did not account for

254 the complete D2 phenotype, including higher frequency loss and disruption of third-row
255 stereocilia in OHCs (Shin et al. 2010). These observations collectively indicate that Fhod3 plays
256 a pivotal role in high-frequency auditory function.
257 Other formin proteins have been associated with hereditary hearing loss, suggesting that altered
258 expression of Fhod3 in our mutant mouse models may contribute to the underlying molecular
259 mechanisms of hearing loss. Mutations in two formin-related hearing loss genes, DIAPH1 and
260 DIAPH3, are predicted to result in a gain-of-function mechanism(Schoen et al. 2010; Ueyama et
261 al. 2016). In line with this, our Fhod3 overexpression mouse model exhibited progressive hearing
262 loss and dominant loss of OHCs in the basal turn region, resembling the DIAPH1 transgenic
263 mice model (Ueyama et al. 2016; Ninoyu et al. 2020). Considering the subcellular localization of
264 Fhod3 primarily in the cuticular plate, and similar phenotypes between loss and overexpression
265 of Fhod3 leading to defective stereocilia bundle structures, we speculate that Fhod3 expression
266 must be tightly modulated to preserve normal cuticular plate and stereocilia structure. The high-
267 frequency range of hearing is particularly susceptible to damage due to its greater mechanical
268 demands but may perhaps also be more generally susceptible to accumulated age-related damage
269 due to higher metabolic requirements (Someya et al. 2010).
270 Significantly, targeted deletion of Fhod3 in conditional knockout mice resulted in a similar
271 phenotype, characterized by elevated ABR thresholds and stereocilia deterioration in the mid-
272 base and base of the cochlea. Even heterozygous mice exhibited progressive hearing loss in the
273 high-frequency range, indicating a dose-dependent effect of Fhod3 expression. Indeed, a Fhod3
274 variant with a missense mutation at a conserved residue in the FH2 domain (Tyr1249A) causes
275 dilated cardiomyopathy by impairing the ability to induce actin dynamics-dependent activation
276 of the transcription factor serum response factor (SRF) (Arimura et al. 2013). These findings are

277 consistent with a critical role for Fhod3 in maintaining actin stoichiometry in the cuticular plate
278 and stereocilia.
279
280 Overall, our study highlights the importance of Fhod3 in regulating actin dynamics and its
281 critical role in maintaining the structural integrity of HCs in the cochlea. These findings provide
282 valuable insights into the pathogenesis of ARHL and open up potential avenues for therapeutic
283 interventions. Further investigations into the molecular mechanisms underlying Fhod3-mediated
284 actin polymerization and its interaction with other proteins involved in hearing loss will deepen
285 our understanding of the disease and pave the way for targeted therapeutic strategies.
286
287

288 **4 Material and Methods**

289 **4.1 Animals**

290 All animal protocols were approved (s17178) by the Institutional Care and Use Committee
291 (IACUC) at University of California San Diego (UC San Diego). C57BL/6J and CBA/J mice used
292 in this study were purchased from Jackson Laboratory (ME, USA).

293 **4.2 Establish Fhod3 over-expression mouse model**

294 We generated a transgenic (TG) mouse model of Fhod3 expressing CAG-loxP-STOP-loxP(LSL)-
295 mouse Fhod3-IRES-GFP. Cochlear RNA was extracted from C57BL/6J mouse with Micro Scale
296 RNA isolation Kit (Ambion) according to the manufacturer's instructions, followed by cDNA
297 synthesis using ProtoScript® Taq RT-PCR Kit [New England Biolabs (NEB), Ipswich, MA, USA].

298 *Fhod3* cDNA was amplified with PrimeSTAR® GXL DNA Polymerase (R050B; Takara Bio, San
299 Jose, CA, USA) using a pair of primers (5'-CACCATGGCCACGCTGGCTTGTCGCGTGCAG-
300 3' for the forward and 5'-GAGCATGCTCACAGTTGCAGTTCAGATGTG -3' for the reverse
301 primer), and subcloned into the pENTR™/D-TOPO™ vector (K2400-20; Thermo Fischer
302 Scientific, Waltham, MA, USA). For the general donor vector, a pair primer (5'-
303 TGCAGGATCCATCGATCACCATGGCCACGCTGGCTTGTCGCGTGCAG-3' for the
304 forward and 5'- CGAGCTCGTCGACGATTCACAGTTGCAGTTCAGATGTG-3' for the
305 reverse primer) was utilized for amplifying *Fhod3* cDNA from the plasmid and this 4.7kb fragment
306 was subsequently cloned into a pGreen-RAGE vector cut with EcoR-V, which includes a
307 CMV/Beta actin Promoter-LSL-MCS-IRES-GFP, by using Gibson Assembly® Cloning Kit (NEB,
308 USA). After confirming the identity of the plasmid by sequencing, the linearized construct was
309 electroporated into mouse embryonic stem cells (mESCs) with a C57BL/6 background.
310 Genotyping was performed using the following primer set; 5'-TGCAGGATCCATCGATCACC-
311 3' and 5'-AACTTCGACCCAACGAGC-3'. Fhod3-overexpression mice were generated by
312 crossing *Tg(Pax2-cre)1Akg/Mmnc* mice(Ohyama and Groves 2004) with the *Fhod3*$^{Tg/+}$.
313

314 **4.3 Generation of hair-cell specific Fhod3 conditional knock-out mouse**

315 HC specific Fhod3 conditional knockout mice (KO) were generated by crossing B6.Cg-*Tg(Atoh1-*
316 *cre)1Bfri/J* mice (The Jackson Laboratory, stock no. 011104) with Fhod3$^{fl/fl}$ mice(Ushijima et al.
317 2018), kindly gifted from Professor Sumimoto at department of Biochemistry, Kyushu University
318 Graduate School of Medical Sciences, Japnan. The Fhod3$^{fl/fl}$ mice contain loxP sites flanking exon
319 18 of the *Fhod3* gene.

320 **4.4 Generation of Fhod3-HA knock-in mice**

321 Using CRISPR/Cas9 editing we generated Fhod3-HA fusion knock-in mice expressing three
322 copies of the human influenza hemagglutinin (HA; TACCCGTATGATGTTCCGGATTACGCT)
323 tag sequence integrated at the C-terminus of Fhod3. Geneious Prime software (Biomatters,
324 Auckland, New Zealand) was utilized to identify the following guide RNA (gRNA) sequences:
325 GCAGTTCAGATGTGCCAACC was located on the last coding exon (exon 28) and
326 GCTGAGCAGAGGACCAGATC was located on the Fhod3 3' untranslated region (3'UTR). For
327 homology-directed repair (HDR), a 1,879 base-pair Fhod3 donor fragment was amplified from
328 mouse genomic DNA by using the following primers (5'-
329 GCCCATAGGAGGGCCTTTACATTTAGTTTTG-3'and 5'-
330 CAGGTGCCTAGAAAGTGACTTAGATTTCCAGG-3'), and cloned into a custom mini-circle
331 compatible hybrid donor plasmid consisting of two U6 promoters (one for each guide) and a
332 docking site for the homology arms and HA tag as previously described (Jurlina et al. 2022).
333 Integration of the amplified mouse genomic DNA into the donor plasmid and integration of the 3x
334 HA tag before the stop codon were each carried out by Gibson assembly (NEB, USA). HDR into
335 C57BL/6J background mouse embryos was carried out by mixing the plasmid donor, guide RNAs
336 [Integrated DNA Technologies (IDT), IA, USA] and Cas9 protein (Alt-R® S.p. HiFi Cas9
337 Nuclease V3; IDT, USA) together and microinjecting into mouse embryos with. For mouse
338 genotyping, following a primer set was used; 5'-GCTTTCCACATAGCACCTACA-3' and 5'-
339 CAGATGTTCAGGTCAAGTCTCC-3'.

340

341 **4.5 Immunofluorescence staining**

342 Mice were anesthetized using an intraperitoneal injection of an anesthetic cocktail (ketamine
343 92.5mg/kg, xylazine 10 mg/kg, and acepromazine 1.85 mg/kg) and fixed via transcardial
344 perfusion with 4% paraformaldehyde (PFA) in 0.1 M phosphate-buffered saline (PBS) (pH 7.4).
345 The cochleae were harvested and post-fixed overnight at 4 °C in 4% PFA in 0.1 M PBS (pH 7.4).
346 After fixation, the cochleae were dissected, and surface preparation was performed. The dissected
347 tissues were permeabilized in PBS with 0.3 % PBST (PBS with 0.3% Triton-X) for 30 min at room
348 temperature, followed by blocking with 10 % normal goat serum (NGS) in 0.03 % PBST for 1 h
349 at room temperature with agitation. Primary antibodies (see below) were applied to the samples in
350 0.03% PBST with 3% NGS and incubated overnight at 4 °C. After washing three times with 0.03%
351 PBST for 10 min each, the tissues were incubated with secondary antibodies in 0.03% PBST with
352 3% NGS for 1 h at room temperature with agitation. The stained tissue was briefly washed with
353 0.03% PBST and mounted in ProLong Antifade (Thermo Fisher Scientific, Cat#P36970, Carlsbad,
354 CA, USA) with a coverslip. Imaging was performed using a confocal microscope with airy-scan
355 processing (LSM880; Carl Zeiss, Jena, Germany).
356 For cryo-sectioning, the fixed cochleae were decalcified in 0.12 M ethylenediaminetetraacetic
357 acid (EDTA) at 4°C for 48 h, followed by cry protection in 30% sucrose at 4°C overnight. The
358 samples were then embedded in O.C.T. compound (Sakura Finetek, CA, USA) and cryo-sectioned
359 into 10 μm thick slices using a cryostat (CM1860; Leica Biosystems, Nussloch, Germany), The
360 sections were mounted on glass slides, and immunofluorescence staining was performed on the
361 glass slide using a hydrophobic barrier pen (IHC World, Cat# SPM0928, MD, USA), as described
362 above.
363
364 **4.6 Antibodies**

365 The following antibodies were used (polyclonal unless indicated): Fhod3 (Thermo Fisher
366 Scientific, Cat# PA5-23313, 1:100); Myo6 (Proteus Bioscience, Cat# 25-6791, 1:250); anti-HA
367 tag (Abcam, Cat# ab9110, 1:100); TuJ-1 monoclonal (R&D systems, Cat# MAB1195, 1:500);
368 Alexa Fluor 568 conjugated phalloidin (Thermo Fischer Scientific, A12380, 1:250); 4'6-
369 diamidino-2-phenylindole (DAPI) (Novus Biologicals, Cat# NBP2-31156, 1:50,000); Alexa Fluor
370 647-conjugated anti-mouse IgG2a (Thermo Fischer Scientific, Cat# A-21241, 1:500); Alexa Fluor
371 488-conjugated anti-rabbit IgG (Themo Fischer Scientific, Cat# A-11008, 1:500).

372 **4.7 Multiplexed error-robust fluorescence *in situ* hybridization (MERFISH)**

373

374 Samples were prepared following the manufacturer's instructions (Vizgen, Cambridge, MA, USA).
375 Briefly, cochleae from postnatal day 5 (P5) C57Bl/6J mice were fixed and cryo-sectioned into 10
376 μm thick slices as described above. RNase inhibitor (NEB, Cat# M0314L, USA) was used to
377 preserve RNA integrity during the dehydration step. The cryosections were placed onto
378 MERSCOPE slide glass (Vizgen, Cat# 20400001, MA, USA) and permeabilized in 70% ethanol
379 at 4 ℃ for 24 hours. Tissues were then incubated with blocking solution (Vizgen, Cat# 20300012,
380 USA) containing cell-boundary staining antibodies (Vizgen, Cat# 20300010 and 20300011, USA)
381 for 1 hour at room temperature. Subsequently, the stained samples were incubated with a
382 customized 140 gene panel mix (Vizgen, Cat# 20300006, USA) including Fhod3 and Myo7a
383 probes for 36 hours at 37 ℃ in a humidified cell culture incubator. After post-encoding
384 hybridization samples were washed with formamide wash buffer (Vizgen, Cat# 20300002, USA),
385 embedded in a polyacrylamide gel incubated with digestion premix (Vizgen, Cat# 20300005,

386 USA), and incubated with clearing premix (Vizgen, Cat# 20300003) until tissues became
387 transparent. Images were acquired and analyzed using the MERSCOPE system (Vizgen, USA).
388 Cell-boundary staining was employed for cell segmentation parameter determination.
389

390 **4.8 Quantitative real-time PCR**

391 Cochleae were harvested at P2 and frozen in liquid nitrogen. Samples were stored at -80 ℃ until
392 following RNA extraction. RNA was isolated with Micro Scale RNA isolation kit (Ambion,
393 Austin, TX, USA) followed by reverse transcription using cDNA synthesis kit (AMIL1791;
394 Ambion, USA). Quantitative real-time PCR (qPCR) was conducted using TaqMan® probe
395 (Fhod3; Mm00614166_m1) obtained from applied biosystems. For each sample, the qPCR assay
396 was performed in triplicate and included the housekeeping gene, GAPDH, as a reference. The
397 relative transcript quantity was determined using the $2^{-\Delta\Delta Ct}$ method, with GAPDH serving as the
398 internal control (Schmittgen and Livak 2008).
399

400 **4.9 Auditory brainstem response**

401 To assess hearing of Fhod3-TG (*Pax2-Cre*$^{+/-}$*; Fhod3* $^{TG/+}$), Fhod3-het (*Atoh1-Cre*$^{+/-}$*; Fhod3*$^{fl/+}$),
402 Fhod3-KO (*Atoh1-Cre*$^{+/-}$*; Fhod3*$^{fl/fl}$) mice and littermate control WT mice, auditory brain stem
403 responses (ABRs) were conducted. Mice were anesthetized with the anesthetic cocktail (ketamine
404 92.5mg/kg, xylazine 10 mg/kg, and acepromazine 1.85 mg/kg), and placed on a heating pad
405 (HP-4M; Physitemp Instruments Inc., Clifton, NJ) regulated by a temperature controller (TCAT-
406 2DF; Physitemp Instruments Inc, NJ). Subcutaneous stainless-steel electrodes were positioned at
407 the vertex of the skull and the right pinna, with the ground electrode placed near the base of the

408 tail. Acoustic stimuli were generated using a PXI data acquisition system (PXI-1031; National
409 Instruments, Austin, TX, USA) and amplified by an SA1 speaker driver (Tucker-Davis
410 Technologies, Alachua, FL, USA). Sound stimuli were presented to the right ear via an 8-inch long
411 plastic tube attached to a custom acoustic system (Eaton-Peabody Laboratories).(Valero et al.
412 2018) ABRs were evoked using 5-msec tone pips with a 30/s presentation rate and a 0.5 msec
413 rise/fall Blackman ramp. The stimuli were delivered at sound pressure levels (SPL) ranging from
414 20 to 100 dB in 5 dB step increments, at frequencies of 4, 8, 16, 24 and 32 kHz. The responses
415 were filtered using a 0.3–3 kHz band-pass filter, amplified by 10,000 times with a P511 pre-
416 amplifier (Grass Instruments, Astro-Med, Inc., RI, USA), and averaged over 512 responses at each
417 dB SPL. The hearing threshold was determined as the lowest sound intensity level at which a
418 recognizable or reproducible wave was observed.

419 **4.10 Quantification of hair cell survival and cuticular plate analysis**

420 The cochleae were immuno-stained with Myo6 and phalloidin, followed by imaging using a 20X
421 objective on an Airyscan confocal microscope (LSM880; Zeiss, Germany) with a pixel size of
422 49nm. Viable hair HCs labeled with Myo6 were manually counted at each cochlear turn: apical
423 (corresponding to the 6-8 kHz region), middle (corresponding to the 12-24 kHz region), and
424 basal (corresponding to the 32-42 kHz region). The survival rate was calculated as the ratio of
425 the number of Myo6-positive HCs to the total number of HCs, including depleted HCs. ImageJ
426 software (available at http://rsb.info.nih.gov/ij; developed by Wayne Rasband, National Institutes
427 of Health, Bethesda, MD, USA) was utilized for the analysis.

428 For the cuticular plate analysis, the average phalloidin intensity at the cuticular plate was
429 measured using ImageJ software. Circular regions of interest (ROIs) were defined at the cuticular

430 plate level adjacent to the stereocilia in outer hair cells (OHC) and inner hair cells (IHC). The
431 same ROIs were applied consistently across experiments. Relative intensity changes were
432 calculated by comparing the phalloidin intensity of the mutants with that of age-matched wild-
433 type (WT) mice.

434 **4.11 Scanning electron microscopy**

435 All animals used in this work were handled following the NIH and UCSD Guidelines for Animal
436 Care as mentioned earlier. Mice were euthanized with CO_2 and decapitated. Inner ears were
437 immediately removed with a fine scissor, transferred to a plastic Petri dish where a small
438 aperture in the bone at the apex region was made with a needle to allow the fixative to flow
439 throughout the whole sensory epithelium. A freshly prepared fixative solution containing 4%
440 formaldehyde [Electron microscopy sciences (EMS)], 2.5% glutaraldehyde (EMS), 100 mM
441 sodium cacodylate buffer (EMS), 2 mM CaCl2 was gently injected into the round window and
442 left for 2 h at room temperature. Then, the cochleae were washed in PBS for 20 min three times,
443 organs of Corti fine dissected under a stereoscope, and transferred to 20-mL glass vials with 100
444 mM sodium cacodylate buffer. Samples were prepared for SEM imaging by OTOT method
445 where two consecutive baths of buffered 1% osmium tetroxide (EMS) and 1% tannic acid
446 (Sigma- Aldrich, St. Louis, MO, USA) were applied for 1 h, with 10 min washes for three times
447 in between. Samples were dehydrated in a graded series of ethanol 200-proof (Thermo Fischer
448 Scientific, USA) till absolute, critical-point dried (Leica EM CPD300; Leica, Wetzlar,
449 Germany), placed on carbon tape onto aluminum stubs, gold-sputtered with ~4 nm thick (Leica
450 EM SCD500; Leica, Germany), and observed in a FEG-SEM (Zeiss Sigma VP; Zeiss,
451 Germany), operated at 5 kV.

452 **4.12 Statistical analysis**

453 All statistical analyses were performed using GraphPad Prism (Prism 9.2.0.; GraphPad Software
454 Inc., La Jolla, CA, USA). All data were presented as mean ± standard deviation or standard error
455 of the mean (SEM). For ABR and survival HCs analysis, two-way analysis of variance (ANOVA)
456 was used to detect significant differences, followed by a Tukey post-hoc test. For others, Mann-
457 Whitney U test was utilized. All statistical details can be found in figure legends. The results were
458 considered statistically significant at $P < 0.05$ (*), $P < 0.01$ (**) and $P < 0.001$ (***).

459

460 **5. Conflicts of Interest**

461 The authors declare no conflict of interests

462

463 **6. Acknowledgement**

464 This study was supported by grants from National Institutes of Health (R01 DC-018566 to
465 R.A.F.). U.M. is supported by NIDCD R21 (DC-018237), NIDCD R01 (DC021075), Core Grant
466 NCI CCSG (CA014195), Nathan Shock Center for Aging Research at the Salk Institute P30
467 AG068635, and a CZI Imaging Scientist Award.

468

469 **7. Authors Contribution**

470 R.A.F and U.M. designed the experiments. E.B. and Y.N. contributed equally as first author.
471 E.B. performed animal studies and some immunofluorescence (IF). Y.N. performed MERFISH,
472 IF, HCs and cuticular plate analysis. E.B. and Y.N. performed all statistical analysis. Q.L. and
473 N.O. designed and generated the TG mice line. Y.N. and K.J.W. designed and established

474 Fhod3-HA mouse line. L.A. performed SEM experiments. Y.N., U.M. and R.A.F. analyzed data

475 and wrote the manuscript.

476

477

8. Reference

Anttonen T, Belevich I, Laos M, Herranen A, Jokitalo E, Brakebusch C, Pirvola U. 2017. Cytoskeletal Stability in the Auditory Organ In Vivo: RhoA Is Dispensable for Wound Healing but Essential for Hair Cell Development. *eNeuro* **4**: ENEURO.0149-17.2017.

Arimura T, Takeya R, Ishikawa T, Yamano T, Matsuo A, Tatsumi T, Nomura T, Sumimoto H, Kimura A. 2013. Dilated Cardiomyopathy-Associated *FHOD3* Variant Impairs the Ability to Induce Activation of Transcription Factor Serum Response Factor. *Circulation Journal* **77**: 2990–2996.

Benkafadar N, François F, Affortit C, Casas F, Ceccato J-C, Menardo J, Venail F, Malfroy-Camine B, Puel J-L, Wang J. 2019. ROS-Induced Activation of DNA Damage Responses Drives Senescence-Like State in Postmitotic Cochlear Cells: Implication for Hearing Preservation. *Mol Neurobiol* **56**: 5950–5969.

Breitsprecher D, Goode BL. 2013. Formins at a glance. *J Cell Sci* **126**: 1–7.

Chen KH, Boettiger AN, Moffitt JR, Wang S, Zhuang X. Spatially resolved, highly multiplexed RNA profiling in single cells. *Science* **348**:aaa6090.

Drummond MC, Belyantseva IA, Friderici KH, Friedman TB. 2012. Actin in hair cells and hearing loss. *Hearing Research* **288**: 89–99.

E Van Eyken 1, G Van Camp, E Fransen, V Topsakal, J J Hendrickx, K Demeester, P Van de Heyning, E Mäki-Torkko, S Hannula, M Sorri, et al. 2007. Contribution of the N-acetyltransferase 2 polymorphism NAT2*6A to age-related hearing impairment. *J.Med. Genet.* **44**:570-8.

Flint J, Eskin E. 2012. Genome-wide association studies in mice. *Nat Rev Genet* **13**: 807–817.

Fransen E, Bonneux S, Corneveaux JJ, Schrauwen I, Di Berardino F, White CH, Ohmen JD, Van de Heyning P, Ambrosetti U, Huentelman MJ, et al. 2015. Genome-wide association analysis demonstrates the highly polygenic character of age-related hearing impairment. *Eur J Hum Genet* **23**: 110–115.

Friedman RA, Van Laer L, Huentelman MJ, Sheth SS, Van Eyken E, Corneveaux JJ, Tembe WD, Halperin RF, Thorburn AQ, Thys S, et al. 2009. GRM7 variants confer susceptibility to age-related hearing impairment. *Hum Mol Genet* **18**: 785–796.

Fujimoto N, Kan-O M, Ushijima T, Kage Y, Tominaga R, Sumimoto H, Takeya R. 2016. Transgenic Expression of the Formin Protein Fhod3 Selectively in the Embryonic Heart: Role of Actin-Binding Activity of Fhod3 and Its Sarcomeric Localization during Myofibrillogenesis. *PLoS One* **11**: e0148472.

Gates GA, Mills JH. 2005. Presbycusis. *The Lancet* **366**: 1111–1120.

513 Ghazalpour A, Rau CD, Farber CR, Bennett BJ, Orozco LD, van Nas A, Pan C, Allayee H,
514 Beaven SW, Civelek M, et al. 2012. Hybrid mouse diversity panel: a panel of inbred
515 mouse strains suitable for analysis of complex genetic traits. *Mamm Genome* **23**: 680–
516 692.

517 Jurlina SL, Jones MK, Agarwal D, De La Toba DV, Kambli N, Su F, Martin HM, Anderson R,
518 Wong RM, Seid J, et al. 2022. A Tet-Inducible CRISPR Platform for High-Fidelity
519 Editing of Human Pluripotent Stem Cells. *Genes* **13**: 2363.

520 Kan-O M, Takeya R, Abe T, Kitajima N, Nishida M, Tominaga R, Kurose H, Sumimoto H.
521 2012. Mammalian formin Fhod3 plays an essential role in cardiogenesis by organizing
522 myofibrillogenesis. *Biol Open* **1**: 889–896.

523 Lavinsky J, Crow AL, Pan C, Wang J, Aaron KA, Ho MK, Li Q, Salehide P, Myint A, Monges-
524 Hernadez M, et al. 2015. Genome-wide association study identifies nox3 as a critical
525 gene for susceptibility to noise-induced hearing loss. *PLoS Genet* **11**: e1005094.

526 Li H, Lu M, Zhang H, Wang S, Wang F, Ma X, Liu J, Li X, Yang H, Shen H, et al. 2022.
527 Downregulation of REST in the cochlea contributes to age-related hearing loss via the
528 p53 apoptosis pathway. *Cell Death Dis* **13**: 1–14.

529 Lynch ED, Lee MK, Morrow JE, Welcsh PL, León PE, King MC. 1997. Nonsyndromic deafness
530 DFNA1 associated with mutation of a human homolog of the Drosophila gene
531 diaphanous. *Science* **278**: 1315–1318.

532 Markaryan A, Nelson EG, Hinojosa R. 2010. Major arc mitochondrial DNA deletions in
533 cytochrome c oxidase-deficient human cochlear spiral ganglion cells. *Acta Oto-*
534 *Laryngologica* **130**: 780–787.

535 Menardo J, Tang Y, Ladrech S, Lenoir M, Casas F, Michel C, Bourien J, Ruel J, Rebillard G,
536 Maurice T, et al. 2012. Oxidative Stress, Inflammation, and Autophagic Stress as the Key
537 Mechanisms of Premature Age-Related Hearing Loss in SAMP8 Mouse Cochlea.
538 *Antioxidants & Redox Signaling* **16**: 263–274.

539 Miyoshi T, Belyantseva IA, Kitajiri S, Miyajima H, Nishio S, Usami S, Kim BJ, Choi BY,
540 Omori K, Shroff H, et al. 2022.Human deafness-associated variants alter the dynamics of
541 key molecules in hair cell stereocilia F-actin cores. *Hum Genet* **141**:363-382

542 Ninoyu Y, Sakaguchi H, Lin C, Suzuki T, Hirano S, Hisa Y, Saito N, Ueyama T. 2020. The
543 integrity of cochlear hair cells is established and maintained through the localization of
544 Dia1 at apical junctional complexes and stereocilia. *Cell Death & Disease* **11**: 1–15.

545 Ohmen J, Kang EY, Li X, Joo JW, Hormozdiari F, Zheng QY, Davis RC, Lusis AJ, Eskin E,
546 Friedman RA. 2014. Genome-wide association study for age-related hearing loss (AHL)
547 in the mouse: a meta-analysis. *J Assoc Res Otolaryngol* **15**: 335–352.

548 Ohyama T, Groves AK. 2004. Generation of Pax2-Cre mice by modification of a Pax2 bacterial
549 artificial chromosome. *genesis* **38**: 195–199.

550 Rau CD, Parks B, Wang Y, Eskin E, Simecek P, Churchill GA, Lusis AJ. 2015. High-Density
551 Genotypes of Inbred Mouse Strains: Improved Power and Precision of Association
552 Mapping. *G3 Genes|Genomes|Genetics* **5**: 2021–2026.

553 Rodríguez-de la Rosa L, Lassaletta L, Calvino M, Murillo-Cuesta S, Varela-Nieto I. 2017. The
554 Role of Insulin-Like Growth Factor 1 in the Progression of Age-Related Hearing Loss.
555 *Frontiers in Aging Neuroscience* **9**.
556 https://www.frontiersin.org/articles/10.3389/fnagi.2017.00411 (Accessed June 7, 2023).

557 Sánchez-Martínez A, Benito-Orejas JI, Tellería-Orriols JJ, Alonso-Ramos MJ. 2017. Autosomal
558 dominant auditory neuropathy and variant DIAPH3 (c.-173C>T). *Acta Otorrinolaringol*
559 *Esp (Engl Ed)* **68**: 183–185.

560 Schmittgen TD, Livak KJ. 2008. Analyzing real-time PCR data by the comparative C(T)
561 method. *Nat Protoc* **3**: 1101–1108.

562 Schoen CJ, Emery SB, Thorne MC, Ammana HR, Śliwerska E, Arnett J, Hortsch M, Hannan F,
563 Burmeister M, Lesperance MM. 2010. Increased activity of Diaphanous homolog 3
564 (DIAPH3)/diaphanous causes hearing defects in humans with auditory neuropathy and in
565 Drosophila. *Proc Natl Acad Sci U S A* **107**: 13396–13401.

566 Schrauwen I, Hasin-Brumshtein Y, Corneveaux JJ, Ohmen J, White C, Allen AN, Lusis AJ, Van
567 Camp G, Huentelman MJ, Friedman RA. 2016. A comprehensive catalogue of the coding
568 and non-coding transcripts of the human inner ear. *Hear Res* **333**: 266–274.

569 Schuknecht HF, Gacek MR. 1993. Cochlear pathology in presbycusis. *Ann Otol Rhinol Laryngol*
570 **102**: 1–16.

571 Shin J-B, Longo-Guess CM, Gagnon LH, Saylor KW, Dumont RA, Spinelli KJ, Pagana JM,
572 Wilmarth PA, David LL, Gillespie PG, et al. 2010. The R109H Variant of Fascin-2, a
573 Developmentally Regulated Actin Crosslinker in Hair-Cell Stereocilia, Underlies Early-
574 Onset Hearing Loss of DBA/2J Mice. *J Neurosci* **30**: 9683–9694.

575 Someya S, Yu W, Hallows WC, Xu J, Vann JM, Leeuwenburgh C, Tanokura M, Denu JM,
576 Prolla TA. 2010. Sirt3 Mediates Reduction of Oxidative Damage and Prevention of Age-
577 Related Hearing Loss under Caloric Restriction. *Cell* **143**: 802–812.

578 Sugiura S, Uchida Y, Nakashima T, Ando F, Shimokata H. 2010. The association between gene
579 polymorphisms in uncoupling proteins and hearing impairment in Japanese elderly. *Acta*
580 *Oto-Laryngologica* **130**: 487–492.

581 Taniguchi K, Takeya R, Suetsugu S, Kan-O M, Narusawa M, Shiose A, Tominaga R, Sumimoto
582 H. 2009. Mammalian formin fhod3 regulates actin assembly and sarcomere organization
583 in striated muscles. *J Biol Chem* **284**: 29873–29881.

584 Ueyama T, Sakaguchi H, Nakamura T, Goto A, Morioka S, Shimizu A, Nakao K, Hishikawa Y,
585 Ninoyu Y, Kassai H, et al. 2014. Maintenance of stereocilia and apical junctional
586 complexes by Cdc42 in cochlear hair cells *J Cell Sci* **127**:2040-52

587 Ueyama T, Ninoyu Y, Nishio S-Y, Miyoshi T, Torii H, Nishimura K, Sugahara K, Sakata H,
588 Thumkeo D, Sakaguchi H, et al. 2016. Constitutive activation of DIA1 (DIAPH1) via C-
589 terminal truncation causes human sensorineural hearing loss. *EMBO Mol Med* **8**: 1310–
590 1324.

591 Ushijima T, Fujimoto N, Matsuyama S, Kan-O M, Kiyonari H, Shioi G, Kage Y, Yamasaki S,
592 Takeya R, Sumimoto H. 2018. The actin-organizing formin protein Fhod3 is required for
593 postnatal development and functional maintenance of the adult heart in mice. *J Biol*
594 *Chem* **293**: 148–162.

595 Valero MD, Hancock KE, Maison SF, Liberman MC. 2018. Effects of cochlear synaptopathy on
596 middle-ear muscle reflexes in unanesthetized mice. *Hearing Research* **363**: 109–118.

597 Van Laer L, Huyghe JR, Hannula S, Van Eyken E, Stephan DA, Mäki-Torkko E, Aikio P,
598 Fransen E, Lysholm-Bernacchi A, Sorri M, et al. 2010. A genome-wide association study
599 for age-related hearing impairment in the Saami. *Eur J Hum Genet* **18**: 685–693.

600

601

602

603 **9. Figures**

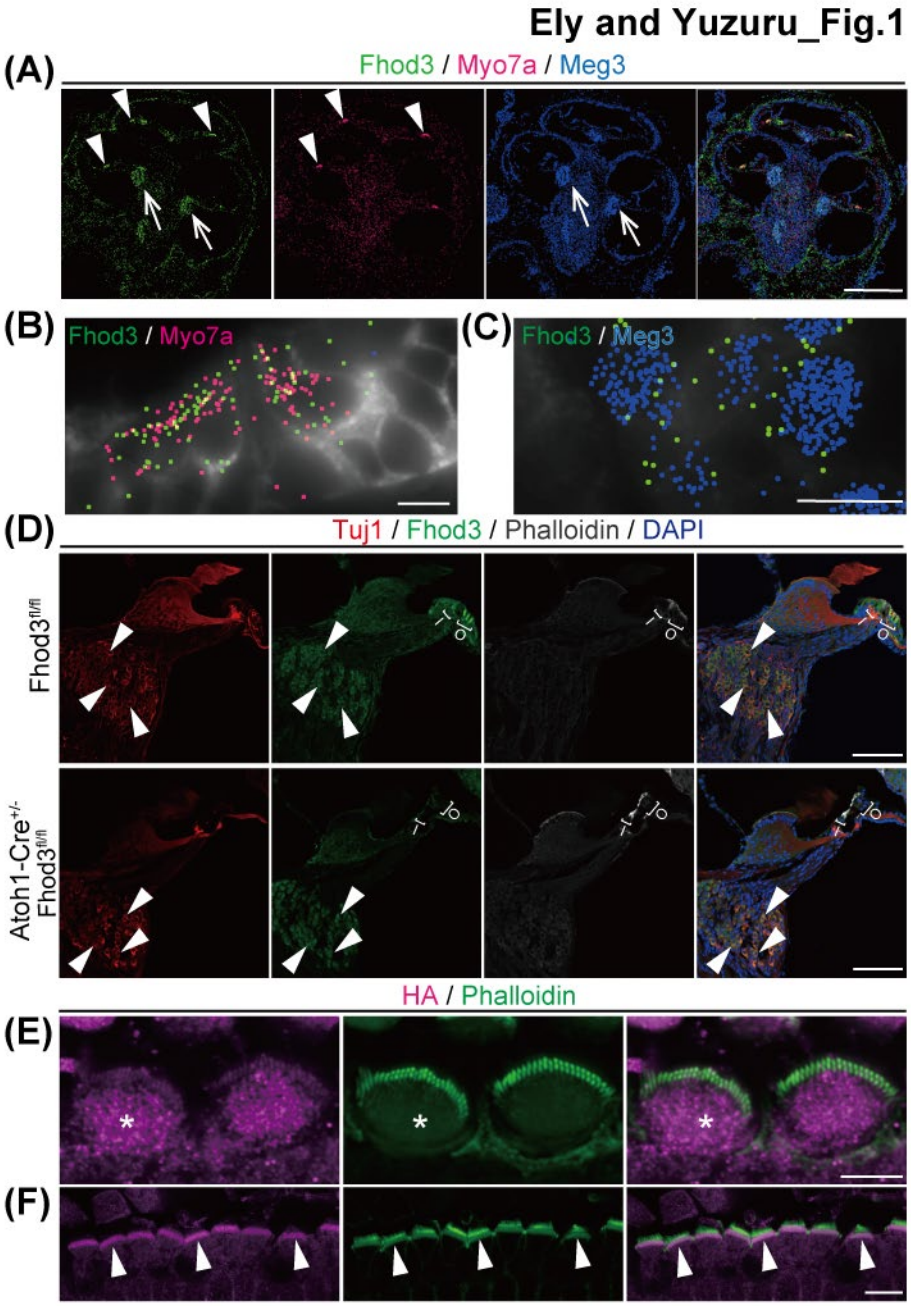

604

605

606 **Fig.1: Cellular and Subcellular localization of Fhod3 in the mouse cochlea**

607 Fhod3 mRNA expression in the mouse cochlea at post neonatal day 5(P5) (A-B). **A)** Multiplexed
608 error robust fluorescent in-situ hybridization (MERFISH) image of the mid modiolar section.
609 Fhod3 transcripts (green) expressed in the hair cell (HC) (arrow head) and spiral ganglion cells
610 (SGCs) (arrow). Myo7a is for HC marker (magenta) and Meg3 (dark blue) is for SGN marker.
611 Scale bar; 500μm. **B-C)** The high magnification image of organ of Corti (B) and spiral ganglion
612 cells (C) of Fig.A. Fhod3 expression was observed in both HCs and SGCs. Cell boundaries were
613 stained with cell boundary staining kit (Vizgen) and depicted by grey color. Scale bar; 25μm. **D)**
614 Cryosections of cochleae of wild type (WT) and Fhod3 knock-out (*Atoh1-Cre*$^{+/-}$*; Fhod3*$^{fl/fl}$) (KO)
615 mice at P14 were stained by Tuj1, Fhod3, phalloidin antibodies and DAPI. Fhod3 expressions
616 were observed in both HCs ant SGCs. Note that Fhod3 signals were diminished in the HC in the
617 KO mouse. Scale bar; 100μm. **E-F)** Outer HCs images at P2 in Fhod3-3xHA knock-in mouse
618 (*Fhod3*$^{HA/+}$). Cochleae were dissected and stained with anti-HA (magenta) and phalloidin (green)
619 antibodies. Fhod3 signals were mainly observed in cuticular plate (asterisk) (E). Lateral view of
620 outer hair cells and arrow heads indicate HA-positive cuticular plate (arrow head) (F). Scale bar:
621 (E) 5μm, (F) 10μm.

622

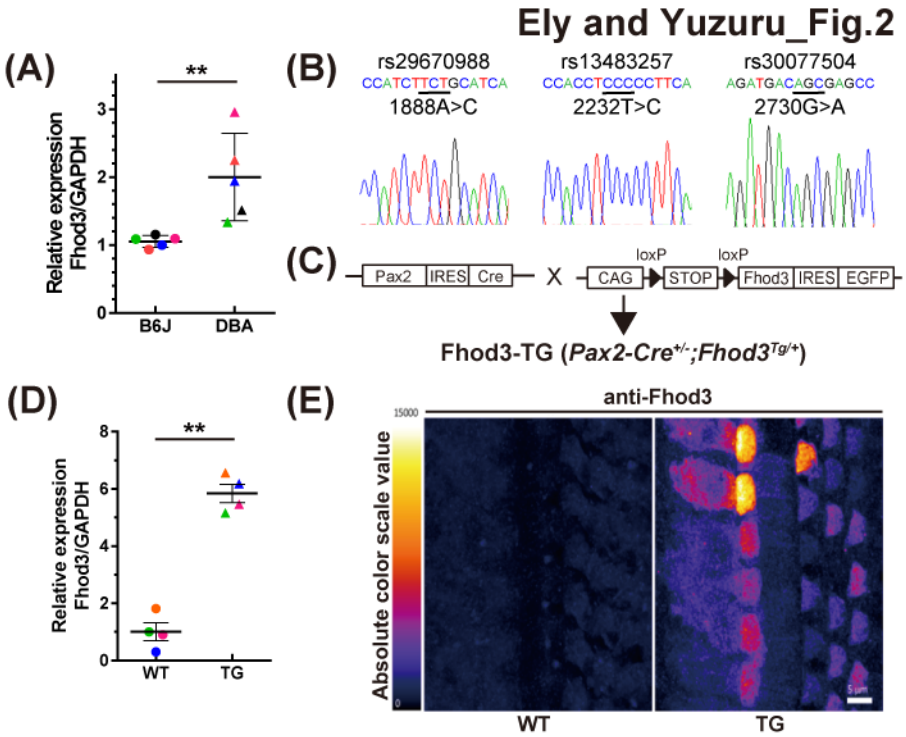
Ely and Yuzuru_Fig.2
(A)
**
Relative expression Fhod3/GAPDH
B6J
DBA
(B)
rs29670988
CCATCTTCTGCATCA
1888A>C
rs13483257
CCACCTCCCCCTTCA
2232T>C
rs30077504
AGATGACAGCGAGCC
2730G>A
(C)
Pax2
IRES
Cre
X
loxP
loxP
CAG
STOP
Fhod3
IRES
EGFP
Fhod3-TG (Pax2-Cre+/-;Fhod3Tg/+)
(D)
**
Relative expression Fhod3/GAPDH
WT
TG
(E)
anti-Fhod3
Absolute color scale value
WT
TG

623

624

625 **Fig.2: Higher expression and nonsense mutations of Fhod3 in the DBA/2J mice and**
626 **generation of Fhod3 transgenic mouse**.

627 **(A)** Comparison of Fhod3 mRNA expression between C57/BL6 (B6) and DBA/2J (D2)
628 mice. Cochlear mRNA was extracted from P2 mice, and Fhod3 and GAPDH were amplified
629 using gene-specific primers. The relative expression level of Fhod3 was calculated. (n=5,
630 Mann-Whitney U test, p^{**}=0.0079).

631 **(B)** Identification of missense mutations in Fhod3 from D2 mice. A comparison of Fhod3
632 sequence cloned from B6 cochlea revealed three non-deleterious mutations: 1888A>C,
633 2232T>C, and 2730G>A. Reference SNP (rs) numbers are indicated, and changed residues
634 are underlined.

635 **(C)** Illustration of the generation of the Fhod3 overexpression mouse model. Fhod3 from B6
636 cochlea was inserted into the CMV/Beta actin Promoter-loxP-STOP-loxP-MCS-IRES-GFP
637 vector, generating a transgenic mouse overexpressing Fhod3 (TG) downstream of the flanked
638 stop codon, controlled by the CMV promoter. The TG mouse was subsequently intercrossed
639 with the Pax2-Cre mouse line to achieve cochlear-specific overexpression of Fhod3 in vivo.

640 **(D)** Relative expression of Fhod3 in wild-type B6 and TG mice. mRNA was obtained from
641 the mice cochleae at P2, and quantitative PCR was performed. Fhod3 expression was
642 normalized to GAPDH. (n=4, Mann-Whitney U test, p^{**}=0.0095).

643 **(E)** Immunofluorescence intensity of Fhod3 in wild-type (WT) and TG mice at P2. The
644 glow-scale bar demonstrates the color gradient of the scale. Scale bar; 5μm.

645

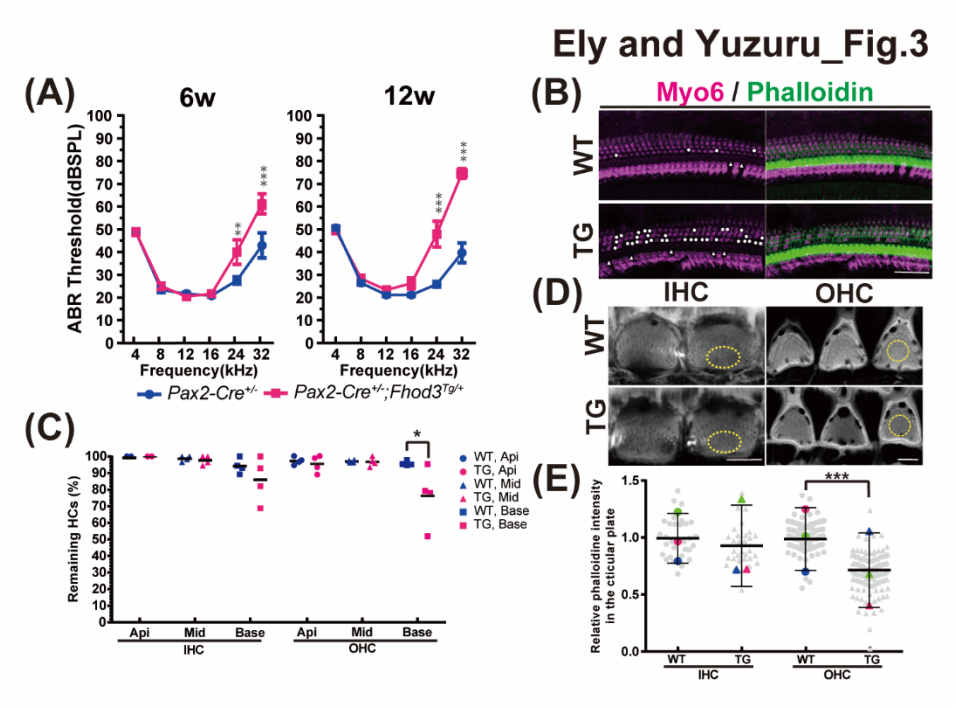
Ely and Yuzuru_Fig.3
(A)
6w
12w
ABR Threshold(dBSPL)
Frequency(kHz)
Pax2-Cre+/-
Pax2-Cre+/-;Fhod3Tg/+
(B)
Myo6 / Phalloidin
WT
TG
(C)
Remaining HCs (%)
WT, Api
TG, Api
WT, Mid
TG, Mid
WT, Base
TG, Base
Api
Mid
Base
IHC
OHC
(D)
IHC
OHC
WT
TG
(E)
Relative phalloidine intensity in the cticular plate
WT
TG
IHC
OHC

646

647

648 **Fig.3 Auditory phenotype and immunohistochemical analysis of Fhod3-TG mice**

649 **(A)** Auditory brainstem response (ABR) thresholds with pure-tone bursts at various
650 frequencies in WT (*Pax2-Cre*$^{-/-}$*; Fhod3*$^{Tg/+}$) and TG (*Pax2-Cre*$^{+/-}$*; Fhod3*$^{Tg/+}$) mice at 6
651 weeks and 12 weeks of age. Significant differences were observed at 24 kHz and 32 kHz,
652 and the thresholds elevation at both frequencies are progressive. Statistical analysis
653 performed using two-way ANOVA followed by a Tukey post-hoc test. (n=12 for each
654 group, p^{**}=0.0097 at 24 kHz (6 weeks), p^{***}<0.0001 at 32 kHz (6 weeks),
655 p^{***}<0.0001 at 24 kHz (12 weeks), p^{***}<0.0001 at 32 kHz (12 weeks)). **(B)**
656 Representative confocal images of the basal turn cochlea at 5 months old, showing
657 immunostaining with Myosin6 and phalloidin. White dots indicate hair cell losses. Scale
658 bar; 20μm. **(C)** Survival hair cell rate in WT and TG mice at 5 months old. The number
659 of surviving Myo6-positive inner and outer hair cells (IHCs and OHCs) was counted, and
660 the survival rate was calculated in the apical (Api), middle (Mid) and basal (Base) turn
661 cochleae. The survival rate of OHC in TG mice at the basal turn cochlea was
662 significantly decreased compared to the WT control (WT vs TG in the basal OHC (%):
663 95.6±0.64 vs 75.93±8.98, p^{*}=0.023 by Mann-Whitney U test, n=4). **(D)**

664 Immunofluorescence images in the cuticular plate of TG mice and the control at 5
665 months old. Phalloidin staining (grey) was performed and show representative images of
666 IHC and OHC in the mid-basal turn cochlea. Region of interests for the measurement of
667 phalloidin intensities are depicted by yellow color dots. Scale bar; 5μm. **(E)** Statistical
668 analysis of phalloidin staining in the cuticular plate at 5 months old. Each grey dots
669 indicates relative phalloidin intensities of remaining hair cells (total n=86, 91, 273 and
670 279), and each colored dots demonstrates average of the intensities per experiment (WT

671 vs TG: (IHC)1.00 ± 0.175 vs 0.92 ± 0.179; (OHC)1.00 ± 0.131 vs 0.70 ± 0.170,

672 p***<0.001, by Mann-Whitney U test, n=3 animals).

673

674

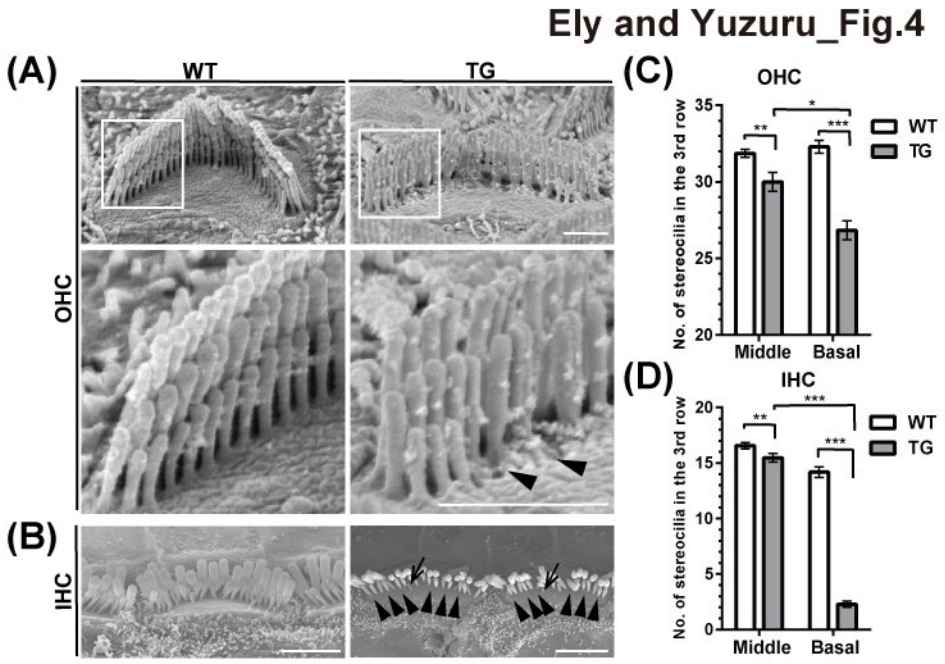

675

676 **Fig.4 Ultrastructural analysis of Fhod3 transgenic mise**

677 Scanning electron microscopy (SEM) images and the comparison of number of stereocilia in
678 the third row of 7-weeks old age cochleae. **(A) (B)** SEM images of outer hair cell (OHC) (A)
679 and inner hair cell (IHC) (B) hair cell stereocilia in WT (*Pax2-Cre*$^{-/-}$*; Fhod3*$^{Tg/+}$) and TG
680 (*Pax2-Cre*$^{+/-}$*; Fhod3*$^{Tg/+}$) mice at basal turn cochleae. White boxed regions are magnified in
681 the lower panel. Arrows indicate missing (arrow head) and remaining (arrow) third row
682 stereocilia in the TG mice. [Scale bar; (A) 1μm, (B) 2.5μm]. **(C)(D)** Comparison of number
683 of stereocilia in the third row of OHC (C) and IHC (D) at middle and basal turn cochleae.
684 Statistical analysis was performed using Mann-Whitney U test. [(C) n=7 for the middle turn
685 (Mid) and the basal turn (Base) cochlea, p*=0.0216 at Mid, p***<0.0001 at Base; (D) n=9
686 and 11 for the Mid, n=15 for the Base, p**=0.0016 at Mid, p***<0.0001 at Base].

687

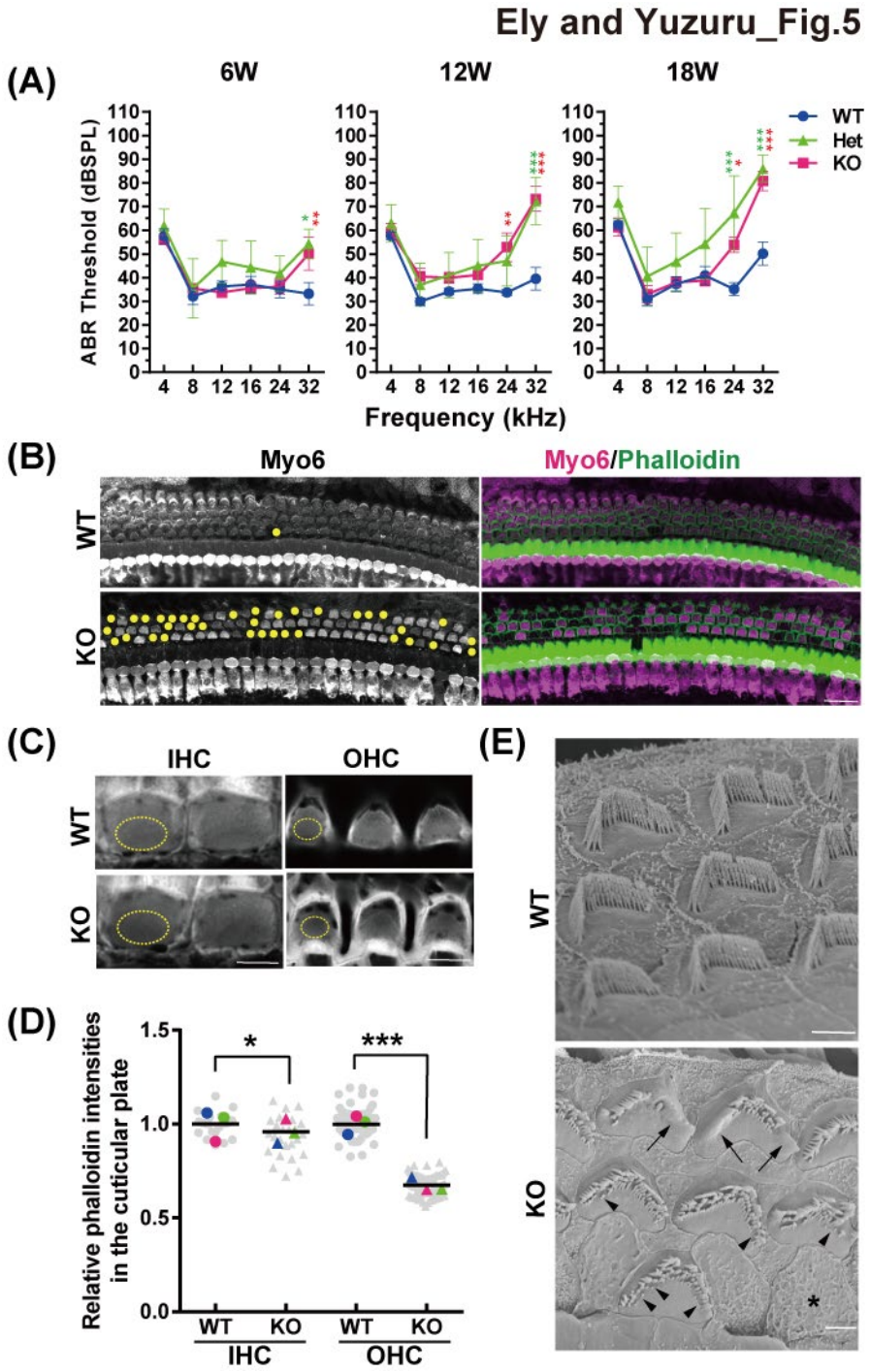
Ely and Yuzuru_Fig.5
(A)
6W
12W
18W
ABR Threshold (dBSPL)
Frequency (kHz)
WT
Het
KO
(B)
Myo6
Myo6/Phalloidin
WT
KO
(C)
IHC
OHC
WT
KO
(D)
Relative phalloidin intensities in the cuticular plate
WT
KO
IHC
OHC
(E)
WT
KO

688

689

690 **Fig.5 Phenotypic analysis of conditional knock-out mouse of Fhod3**

691 **(A)** ABR measurements of wild type (WT) (*Math1-Cre*$^{-/-}$*; Fhod3*$^{fl/fl}$) (n=16), heterozygous
692 (Het) (*Math1-Cre*$^{+/-}$*; Fhod3*$^{fl/+}$) (n=4), knock-out (KO) (*Math1-Cre*$^{+/-}$*; Fhod3*$^{fl/fl}$) (n=9)
693 mice at 6, 12 and 18 weeks of age. Two-way ANOVA was used to detect significant
694 differences, followed by a Tukey post-hoc test. $p^{*}<0.05$, $p^{**}<0.01$, $p^{***}<0.001$.

695 **(B)** Immunohistochemical analysis was conducted on WT and KO mice cochleae from the
696 basal turn cochlea at 3 months of age. Cochleae were harvested, fixed and stained with
697 Myo6 and phalloidin. Heir cell losses were represented by yellow dots. Scale bar;20μm.

698 **(C)** Representative images of cuticular plate with phalloidin staining in WT and KO mice in
699 the mid-basal turn cochlea at 3-months old. Region of interests for the following
700 phalloidin staining analysis (D) are depicted (yellow dots). Scale bar; 5μm.

701 **(D)** Statistical analysis of phalloidin staining in the cuticular plate at 3-months old. Each
702 grey dots indicates relative phalloidin intensities of survival hair cells (total n=86, 91,
703 273 and 279), and each colored dots demonstrates average of the intensities per
704 experiment ($p^{***}<0.001$ by Mann-Whitney U test, n=3 animals).

705 **(E)** SEM images of OHC of WT and KO in the mid-basal-turn cochlea at 3-months old.
706 Abnormal fused stereocilia (arrow), short and missing stereocilia in the third row (arrow
707 head) and complete loss of stereocilia (asterisk) in KO mice are indicated. Scale bar;
708 2μm.